Phononic band gaps induced by inertial amplification in periodic media

C. Yilmaz,* G. M. Hulbert, and N. Kikuchi
Department of Mechanical Engineering, University of Michigan, Ann Arbor, Michigan 48109-2125, USA
(Received 24 April 2007; revised manuscript received 11 July 2007; published 28 August 2007)

In the literature, phononic band gaps in periodic media are generated via two different means, namely, Bragg scattering and local resonances. In this paper, an alternative method is introduced, in which effective inertia of the wave propagation medium is amplified via embedded amplification mechanisms. A prototype two-dimensional mass-spring lattice is introduced. The band structure of this lattice is computed for various instantiations to highlight the benefits of inertial amplification and to quantify the sensitivity of inertial amplification induced band gaps to parametric variations. It is shown that inertial amplification gives rise to very wide band gaps at low frequencies.

DOI: 10.1103/PhysRevB.76.054309 PACS number(s): 62.30.+d, 63.20.Dj, 46.40.−f, 46.40.Cd

I. INTRODUCTION

Spectral gaps in the band structure of periodic media have long been attracting many researchers.[1] In the last decade, there has been growing interest in computing and designing the phononic band structure of two- and three-dimensional periodic systems comprising various materials.[2–7] Of particular focus has been obtaining complete phononic band gaps, which forbid the propagation of elastic or acoustic waves regardless of mode or wave vector. Practical applications of these systems include mechanical filters, sound and vibration isolators, and acoustic waveguides.[7,8]

There are two different widely published means of generating phononic band gaps in periodic media, which are Bragg scattering and local resonances.[5,9,10] In Bragg scattering, a gap appears due to destructive interference of the wave reflections from the periodic inclusions within the media. Band gaps can also be generated via local resonators, which impede wave propagation around their resonance frequencies. Moreover, a band gap can be formed by the combined effect of these two mechanisms.[5,9,10]

A significant and practical challenge is to design solid systems that possess wide low-frequency band gaps. Due to the existence of transverse (shear) modes in solids, it is harder to obtain wide low-frequency band gaps when compared to fluids.[11] Moreover, the lowest frequency gap due to Bragg scattering is of the order of the wave speed (longitudinal or transverse) of the medium divided by the lattice constant.[10,13] Thus, to have a low-frequency Bragg gap, one needs low wave speeds (i.e., heavy inclusions in a soft medium) or a large lattice constant. Heaviness, low stiffness, and large size are not good attributes for band gap structures that are to be used for practical purposes. On the other hand, by choosing low resonator frequencies, one can place local resonator induced band gaps at much lower frequencies than that can be obtained by Bragg scattering.[12–15] Low-frequency local resonances can be realized by embedding rubber-coated dense metal (e.g., Pb or Au) spheres or cylinders in an epoxy matrix.[10,12,13] It has been shown that the gap size and the gap center frequency are independent of the geometric arrangement of the coated inclusions (local resonators) within the medium but are dependent on their volume filling fraction.[10] Moreover, to obtain wide band gaps at low frequencies, large volume filling fractions are required.[10,13] Since the average density of the coated inclusions, i.e., rubber and dense metal, is more than the epoxy matrix, large volume fractions imply even larger mass fractions. Therefore, to obtain wide band gaps at low frequencies, one needs heavy resonators that form a large fraction of the overall mass of the medium.

In this paper, phononic band gaps are generated via an alternate method, in which effective inertia of the wave propagation medium is amplified via embedded amplification mechanisms. One of the first designs that made use of amplified effective inertia employs a single stage vibration isolator consisting of a levered mass in parallel with a spring.[16] These systems are used to isolate massive objects from vibrations. The lever in the system generates large inertial forces by amplifying the motion of a small mass, which in turn effectively increases the inertia of the overall system by lowering its resonance frequency. Furthermore, the isolator also introduces an antiresonance frequency when the inertial force generated by the levered mass cancels the spring force. For a literature review on vibration isolation systems that utilize this principle, see Yilmaz and Kikuchi.[17] In the present paper, this inertial amplification method is utilized to generate band gaps in infinite periodic systems. The amplification mechanisms in consideration are not in the form of levers, but their simple yet effective geometry allows them to be easily embedded into two- or three-dimensional lattices. To illustrate the band gaps generated by inertial amplification, a two-dimensional mass-spring lattice is considered, which can sustain in-plane waves with longitudinal and transverse modes. The characteristics of the gaps obtained via this method are determined and compared with those obtained via Bragg scattering and local resonators. The presented method gives rise to very wide band gaps at low frequencies even in the presence of transverse modes. Furthermore, wide low-frequency band gaps can be realized without using large mass fractions on the embedded amplifiers.

II. LATTICE WITH INERTIAL AMPLIFICATION

Consider the system in Fig. 1. First, we assume that the springs k_a are rigid. In this case, when the masses m are displaced by a small amount u toward each other, m_a is displaced by an amount $u/\tan(\theta)$. If θ is small (not infinitesi-

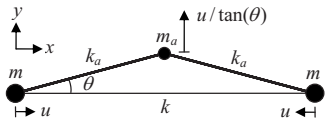

FIG. 1. The system with amplification mechanism. Here, the thin line is an axial spring with stiffness k, and the thick lines are axial springs each with stiffness k_a. The big and small dots represent point masses with masses m and m_a, respectively. Within the system, the springs k_a and the mass m_a form the amplification mechanism.

mally small), then the displacements of the masses m will cause amplified displacement for the mass m_a with an amplification ratio of $1/\tan(\theta)$. As there is only one nonzero mode of vibration, the corresponding equation of motion is given by

$$\left(2m + \frac{m_a}{\tan(\theta)^2}\right)\ddot{u} + 4ku = 0. \tag{1}$$

In Eq. (1), the term that multiplies $\ddot{u}$ is the effective inertia of the system. Statically, the total mass of the system is $2m + m_a$. However, the effective inertia can be much larger than the total mass by prescribing small values of θ. Amplification of inertia is possible due to the amplified inertial forces generated by the mass m_a. If the springs k_a are not rigid, then there will be two additional degrees of freedom in the system. Amplified inertial forces can still be generated if the system is excited at a frequency less than the resonance frequencies caused by the finite stiffness amplification mechanism. Therefore, inertial amplification effect is present until resonance effect takes place.

A two-dimensional infinite periodic lattice, using the amplification mechanism of Fig. 1, is shown in Fig. 2(a). The wave propagation characteristics of this lattice are determined from the irreducible unit cell shown in Fig. 2(b) via Bloch's theorem.[18–20] In this lattice, the thin lines with stiffness k and big dots with mass m form a triangular truss structure. To form the lattice, the thick lines with stiffness k_a and the small dots with mass m_a are added to this truss structure. These additions do not increase the static stiffness of the system since they form mechanisms. We denote the nodes with mass m as structural nodes, since they make up the structural backbone of the lattice. If the springs denoted by k_a are assumed to be rigid, the motion of the masses m_a will be rigidly coupled to the masses m. If θ is small (not infinitesimally small), then the relative displacements of the structural nodes will cause amplified displacements for the masses m_a. Consequently, the lattice possesses inertial amplification.

To see the effect of inertial amplification on the generation of band gaps, we derive the dispersion equation of the lattice for the general case of finite k_a, which can be set to a very large value to approximate rigid coupling. The derivation can be found in Appendix A, which gives the dispersion equation of the lattice as

$$\det(\mathbf{K}(\boldsymbol{\gamma}) - \omega^2\mathbf{M}) = 0. \tag{2}$$

To obtain the band structure of the lattice, Eq. (2) is solved for ω by evaluating $\boldsymbol{\gamma}$ on the exterior boundary of the irreducible Brillouin zone shown in Fig. 2(c) along the path Γ-M-K-Γ. If all the parameter values are finite and nonzero, the dispersion relation $\omega(\boldsymbol{\gamma})$ has 14 branches. Otherwise, there are less number of branches corresponding only to the finite and nonzero frequency modes. Plotting $\omega(\boldsymbol{\gamma})$ reveals the band structure in which only complete band gaps will be considered, i.e., the frequency ranges in which no branch exists regardless of mode.

III. NUMERICAL RESULTS

The band structure of the lattice described in the previous section is computed for several different instantiations. In the first case, parameter values are prescribed such that the lattice comprises only the structural backbone, i.e., no amplification mechanism exists. This baseline configuration is then contrasted with a model in which rigid mechanisms are introduced, followed by a model in which the mechanism springs are compliant. To isolate the effect of inertial amplification, an additional kinematic constraint is embedded on the mechanism pairs. Finally, the sensitivity of the inertial amplification induced band gaps to variations of the lattice parameters is demonstrated.

A. Lattice without amplification mechanisms

As a baseline configuration, consider the lattice in Fig. 2 without amplification mechanisms added. To this end, let $k=1$, $m=1$, $k_a=0$, $m_a=0$, and $\theta=0$ (numerically, m_a is as-

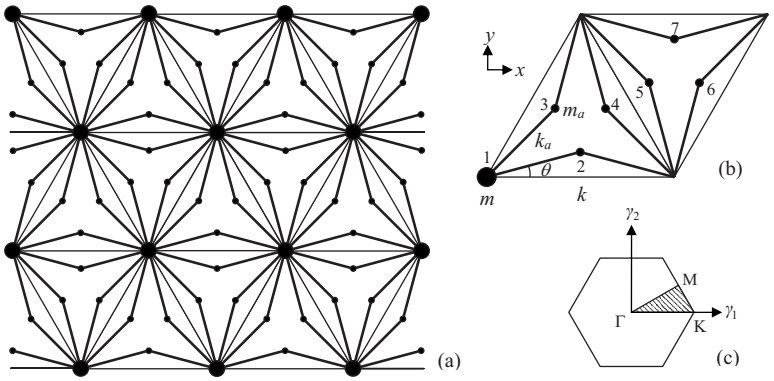

FIG. 2. (a) The infinite periodic lattice with inertial amplification and (b) its irreducible unit cell. Here, the thin lines with stiffness k and big dots with mass m form a triangular truss structure. The thick lines with stiffness k_a and the small dots with mass m_a form the amplification mechanisms. The angle θ determines the amplification generated by the mechanisms. The numbers 1–7 denote the nodes within the unit cell. (c) The hexagonal first Brillouin zone of the reciprocal lattice, in which the irreducible Brillouin zone is shaded. The hexagon has side length $4\pi/3l$.

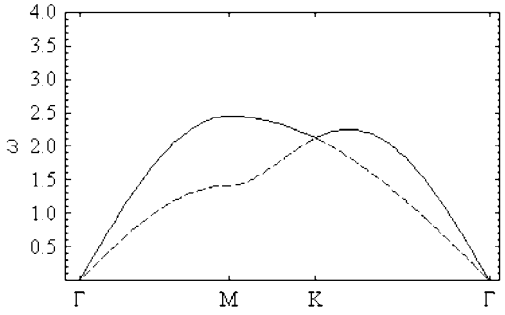

FIG. 3. Band structure of the lattice for $k=1$, $m=1$, $k_a=0$, $m_a=0$, and $\theta=0$. Longitudinal and transverse branches are represented with continuous and dashed lines, respectively.

signed a very small value to preserve the rank of the mass matrix). In this case, we are left with the triangular truss structure that forms the backbone of the lattice. Figure 3 shows the computed band structure. There are only two branches and no gap between them. However, the lattice is a low-pass system, and there is a semi-infinite gap starting at $\omega=2.449$.

B. Lattice with rigid amplification mechanisms

To see the effect of inertial amplification, we set the overall mass of the unit cell, i.e., $m+6m_a$, again equal to 1 but assign half the mass on rigid amplification mechanisms. To this end, let $k=1$, $m=0.5$, $k_a\to\infty$, $m_a=0.5/6$, and $\theta=\pi/18$ (numerically, k_a is assigned a very large value). Figure 4 shows the band structure of this case. Again, only two branches and a semi-infinite gap exist. However, due to inertial amplification, the gap starts at $\omega=0.830$, which is one-third of the previous case.

In Figs. 3 and 4, the slopes of the transverse and the longitudinal branches in the long wavelength limit give the transverse and the longitudinal wave speeds, c_t and c_l, respectively. For both cases, $c_t=0.612l$ and $c_l=1.061l$, where l is the lattice constant. In general, c_t and c_l can be determined in terms of k, m, m_a, and l. We denote the first two branches of $\omega(\boldsymbol{\gamma})$ as ω_1 and ω_2 in increasing order. If $m_a=0$, then the 14×14 system in Eq. (2) is reduced to a 2×2 system that

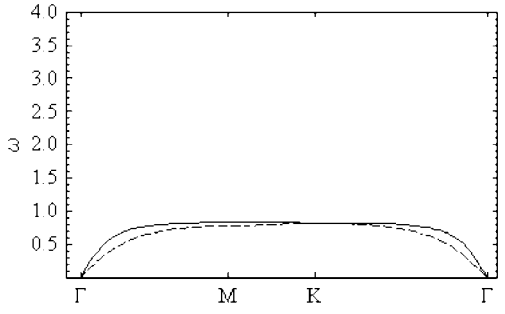

FIG. 4. Band structure of the lattice for $k=1$, $m=0.5$, $k_a\to\infty$, $m_a=0.5/6$, and $\theta=\pi/18$. Longitudinal and transverse branches are represented with continuous and dashed lines, respectively.

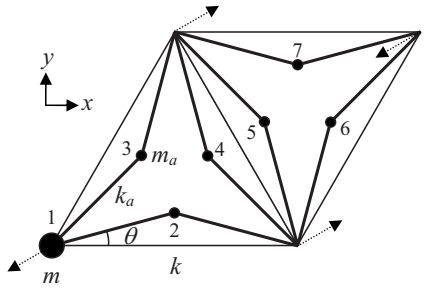

FIG. 5. Displacements of the structural nodes when the wave vector $\boldsymbol{\gamma}$ is at point M in the Brillouin zone. All these displacements denoted by dotted arrows have the same amplitude u.

can be solved analytically for ω_1 and ω_2. Let $\gamma(\phi)$ be the magnitude of $\boldsymbol{\gamma}=(\gamma_1,\gamma_2)$ in the propagation direction $\phi=\tan^{-1}(\gamma_2/\gamma_1)$; then,

$$c_t(\phi)=\lim_{\gamma(\phi)\to0}\frac{\partial\omega_1}{\partial\gamma(\phi)},\quad c_l(\phi)=\lim_{\gamma(\phi)\to0}\frac{\partial\omega_2}{\partial\gamma(\phi)}. \tag{3}$$

Owing to the isotropy of the lattice, for any ϕ, Eq. (3) yields the wave speeds for the 2×2 system as $c_t=l\sqrt{3k/8m}$ and $c_l=l\sqrt{9k/8m}$. For the general 14×14 system with $m_a\neq0$, the addition of the amplification mechanisms does not change the static stiffness regardless of the value of k_a; however, the unit cell mass becomes $m+6m_a$. As a result, the wave speeds for the 14×14 system are

$$c_t=l\sqrt{3k/8(m+6m_a)},\quad c_l=l\sqrt{9k/8(m+6m_a)}. \tag{4}$$

Therefore, if k and $m+6m_a$ are equal for two lattices, then the wave speeds are the same, which can be seen by comparing the cases in Figs. 3 and 4.

The highest frequency in the lattice, which is also the starting frequency of the semi-infinite gap, is obtained when the wave vector $\boldsymbol{\gamma}$ is at point M in the Brillouin zone. Figure 5 shows the displacements of the structural nodes, when the wave vector $\boldsymbol{\gamma}$ is at this point. Using the displacements of the structural nodes, we formulate the starting frequency of the semi-infinite gap denoted as ω_s in terms of k, m, m_a, and θ as $k_a\to\infty$ (see Appendix B for details). The outcome is as follows:

$$\omega_s^2=\frac{6k}{m_a\left(\frac{3}{\tan(\theta)^2}+\tan(\theta)^2+2\right)+m}. \tag{5}$$

In the lattice, changing k and the overall mass of the unit cell $(m+6m_a)$ scales the wave speeds c_l and c_t as seen in Eq. (4). Thus, the normalized gap starting frequency $\omega_s l/2\pi c_t$ can be written in terms of just θ and the mass fraction on amplifiers, given by

$$\mu=6m_a/(m+6m_a). \tag{6}$$

Using Eq. (4) in Eq. (5) yields

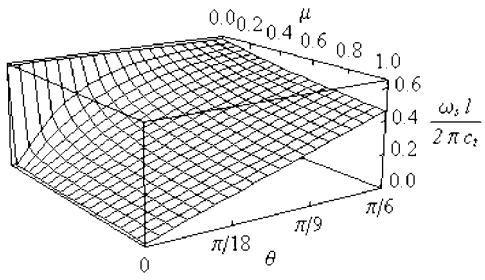

FIG. 6. Normalized gap starting frequency ($\omega_s l/2\pi c_t$) as a function of θ and the mass fraction on amplifiers (μ).

$$\frac{\omega_s l}{2\pi c_t} = \frac{2/\pi}{\sqrt{\mu\left(\frac{1}{2\tan(\theta)^2} + \frac{\tan(\theta)^2}{6} - \frac{2}{3}\right) + 1}}. \quad (7)$$

Figure 6 shows the dependence of $\omega_s l/2\pi c_t$ on θ and μ. When μ is zero, the lattice becomes the triangular truss structure with a normalized gap starting frequency of 0.637, which is the upper bound. By increasing μ and/or prescribing small θ values, much lower gap starting frequencies are obtained. Note that $\omega_s l/2\pi c_t$ remains relatively constant along the μ axis if μ is not close to zero. Thus, the amplifier mass fraction does not need to be very large to generate low gap starting frequencies, provided that amplification is large (i.e., θ is small).

C. Lattice with finite stiffness amplification mechanisms

In this section, inertial amplification is engendered using stiff, but not rigid, amplification mechanisms. Consider $k=1$, $m=0.5$, $k_a=10$, $m_a=0.5/6$, and $\theta=\pi/18$. Figure 7(a) shows the band structure for this case. There are two flat branches (each composed of four coinciding branches) at $\omega=\sin(\theta)\sqrt{2k_a/m_a}=2.690$ and $\omega=\cos(\theta)\sqrt{2k_a/m_a}=15.26$ corresponding to the transverse and longitudinal resonance modes of the amplification mechanisms, respectively. Overall, there are four band gaps between the branches. The semi-infinite gap above all the branches is not of concern. Table I shows the lower and upper limits for the gaps and the normalized gap widths, i.e.,

$$\Delta\omega/\omega_g = (\omega_u - \omega_l)/\omega_g, \quad \omega_g = (\omega_u + \omega_l)/2, \quad (8)$$

where ω_l and ω_u correspond to the lower and upper band gap limits, respectively, and ω_g is the midgap frequency.

Note that the band structure in Fig. 7(b) is similar to the one in Fig. 4. The lower limit of the first band gap in Fig. 7(b), i.e., $\omega=0.795$, is a little bit smaller than that of the semi-infinite gap in Fig. 4, which was $\omega=0.830$. The slight reduction in the lower limit is due to the finite stiffness of the amplification mechanisms. Besides, due their finite stiffness, transverse resonance modes of the amplification mechanisms set the upper limit for the first band gap.

The inertial amplification effect in the lattice can be removed by placing rigid links between the neighboring amplification mechanisms (see Fig. 8). In this case, the springs k_a and the masses m_a cannot form mechanisms anymore, but

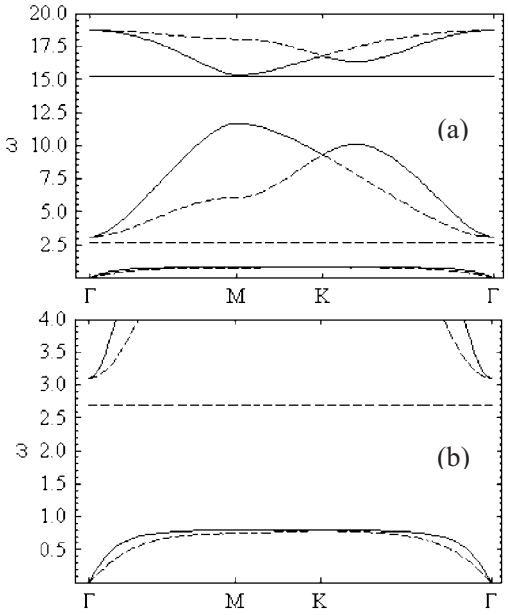

FIG. 7. (a) Band structure of the lattice for $k=1$, $m=0.5$, $k_a=10$, $m_a=0.5/6$, and $\theta=\pi/18$. (b) Details of the band structure in the lower frequency range. Longitudinal and transverse branches are represented with continuous and dashed lines, respectively. The flat branches correspond to the longitudinal (continuous line) and transverse (dashed line) resonance modes of the amplification mechanisms.

they become part of the structural backbone. However, the masses m_a can displace in transverse and longitudinal directions relative to the edges that they span. The dispersion equation for this case can be obtained by adding new coupling terms to the equations of motion of the original lattice. Figure 9(a) shows the band structure of this system. Again, there are two flat branches at $\omega=\sin(\theta)\sqrt{2k_a/m_a}=2.690$ and $\omega=\cos(\theta)\sqrt{2k_a/m_a}=15.26$, corresponding to the transverse and longitudinal resonance modes of the masses m_a with respect to the edges that they span. The band structure is very similar to the one of Fig. 7(a), except that the first gap in Fig. 7(a) does not exist, which can be seen more clearly by comparing Figs. 7(b) and 9(b). Thus, the origin of the first gap in Fig. 7(a) is inertial amplification. Moreover, due to the unaltered local resonances of the masses m_a in the transverse direction with respect to the edges that they span, the second gap in Fig. 7(a) remains unchanged in Fig. 9(a). This local resonance induced gap is the lowest frequency gap in the

TABLE I. Lower (ω_l) and upper (ω_u) band gap limits and normalized gap widths ($\Delta\omega/\omega_g$) for $k=1$, $m=0.5$, $k_a=10$, $m_a=0.5/6$, and $\theta=\pi/18$.

Gap No.	ω_l	ω_u	$\Delta\omega/\omega_g$
1	0.795	2.690	1.088
2	2.690	3.101	0.142
3	11.65	15.26	0.268
4	15.26	15.35	0.006

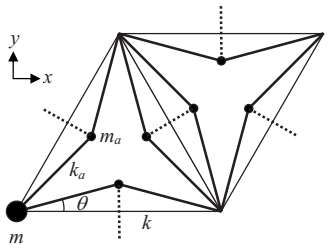

FIG. 8. The modified unit cell. Here, rigid links (as shown by dotted lines) are placed between the neighboring amplification mechanisms in order to eliminate the inertial amplification effect.

lattice without inertial amplification. The higher frequency gaps are not of practical concern, since the major challenge is to obtain large low-frequency band gaps.

Again, consider the original lattice with inertial amplification. Now, we investigate the effect of using a small value for k_a. For this purpose, let $k=1$, $m=0.5$, $k_a=0.1$, $m_a=0.5/6$, and $\theta=\pi/18$. Figure 10(a) shows the band structure of this case. There are again two flat branches, now at $\omega=\sin(\theta)\sqrt{2k_a/m_a}=0.269$ and $\omega=\cos(\theta)\sqrt{2k_a/m_a}=1.526$, corresponding to the transverse and longitudinal resonance modes of the amplification mechanisms, respectively. Again, there are four band gaps between the branches. Table II shows the lower and the upper limits for the gaps and the normalized gap widths. The normalized width of the first gap, which arises from inertial amplification, is reduced significantly compared to the case with $k_a=10$ (see Table I).

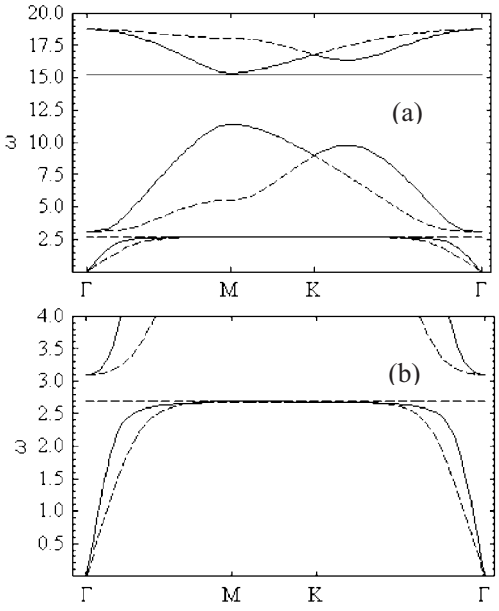

FIG. 9. (a) Band structure of the modified lattice (with rigid links between the neighboring amplification mechanisms) for $k=1$, $m=0.5$, $k_a=10$, $m_a=0.5/6$, and $\theta=\pi/18$. (b) Details of the band structure in the lower frequency range. Longitudinal and transverse branches are represented with continuous and dashed lines, respectively. The flat branches correspond to the longitudinal (continuous line) and transverse (dashed line) resonance modes of the masses m_a with respect to the edges that they span.

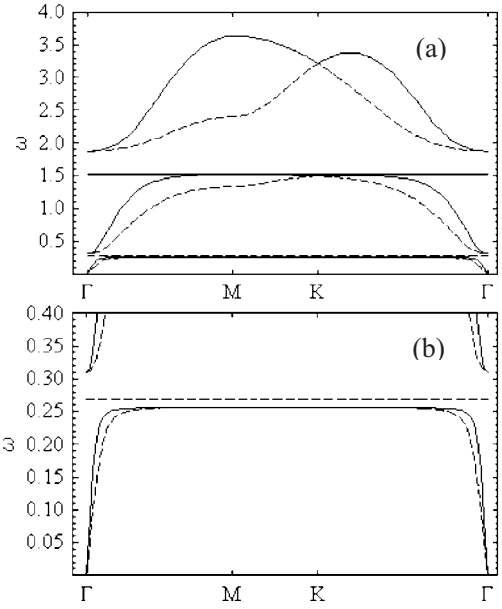

FIG. 10. (a) Band structure of the lattice for $k=1$, $m=0.5$, $k_a=0.1$, $m_a=0.5/6$, and $\theta=\pi/18$. (b) Details of the band structure in the lower frequency range. Longitudinal and transverse branches are represented with continuous and dashed lines, respectively. The flat branches correspond to the longitudinal (continuous line) and transverse (dashed line) resonance modes of the amplification mechanisms.

However, the normalized width of the second gap, which is due to local resonance, did not change. Reducing k_a reduces the midgap frequencies of both of these gaps.

Now, we consider the effect of the lattice parameters on the frequency limits of the first band gap, which arises from inertial amplification. To this end, normalized frequencies $\omega l/2\pi c_t$ are considered, which enables us to fully characterize the first band gap by θ, the stiffness ratio k_a/k, and the mass fraction μ.

First, we consider the effect of the stiffness ratio k_a/k on the frequency limits of the first band gap. To this end, let $\mu=0.5$, $\theta=\pi/18$, and vary k_a/k from 1 to 100. As seen in Fig. 11(a), the lower limit of the gap remains relatively constant, except for small k_a/k values. The upper limit of the gap increases proportionally to $\sqrt{k_a/k}$. As seen in Fig. 11(b), one does not need very large k_a/k values to obtain wide gaps.

These results show that band gap size can be increased by increasing the stiffness ratio k_a/k. The gap size increase is

TABLE II. Lower (ω_l) and upper (ω_u) band gap limits and normalized gap widths ($\Delta\omega/\omega_g$) for $k=1$, $m=0.5$, $k_a=0.1$, $m_a=0.5/6$, and $\theta=\pi/18$.

Gap No.	ω_l	ω_u	$\Delta\omega/\omega_g$
1	0.257	0.269	0.047
2	0.269	0.310	0.142
3	1.525	1.526	0.0006
4	1.526	1.872	0.204

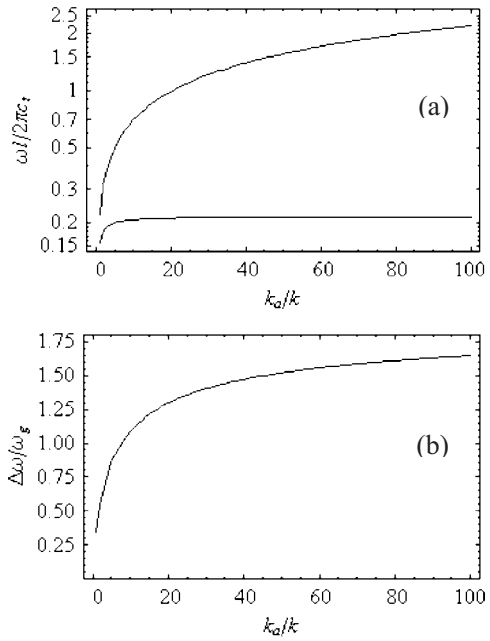

FIG. 11. (a) Upper and lower band gap limits of the first band gap in the lattice with inertial amplification for $\mu=0.5$ and $\theta=\pi/18$ as a function of the stiffness ratio k_a/k. (b) Normalized gap width as a function of k_a/k.

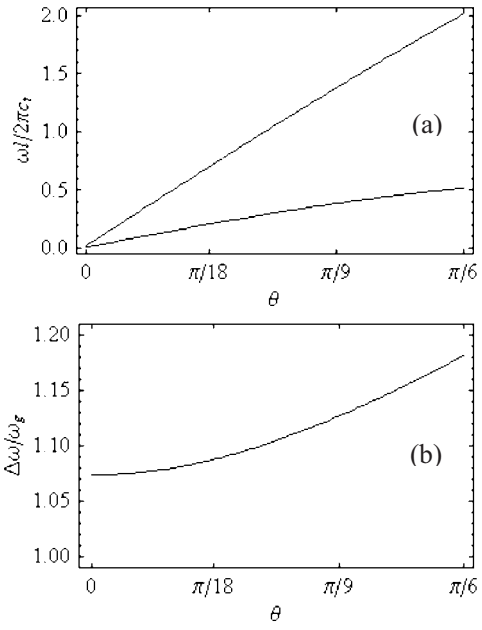

FIG. 12. (a) Upper and lower band gap limits of the first band gap in the lattice with inertial amplification for $\mu=0.5$ and $k_a/k=10$ as a function of θ. (b) Normalized gap width as a function of θ.

accompanied by an increase in the midgap frequency. To lower the midgap frequency, amplification within the lattice can be increased by reducing θ. To observe this effect, let $\mu=0.5$, $k_a/k=10$, and vary θ from $\pi/600$ to $\pi/6$ (very small θ values resulting in extremely large amplifications, which may not be realized physically, are included to show the trend in the limit when θ approaches zero). As seen in Fig. 12(a), when θ approaches zero, both the upper and the lower limits of the first band gap approach zero, while the normalized gap width does not change much [see Fig. 12(b)]. Therefore, as long as large amplifications are realized, midgap frequency of inertial amplification induced band gaps can be much smaller than 1 in terms of normalized frequencies. This is in contrast to obtaining band gaps via Bragg scattering, in which the midgap frequency of the lowest gap can be on the order of 1 in terms of normalized frequencies.

Finally, we investigate the effect of mass distribution within the unit cell on the upper and the lower limits of the first band gap. To this end, let $k_a/k=10$, $\theta=\pi/60$, and vary μ from 0 to 1. Figure 13(a) shows that when the mass fraction on amplifiers (μ) increases, both the upper and the lower limits decrease with a decreasing rate. Moreover, as seen in Fig. 13(b), the normalized gap width remains nearly constant except for small mass fractions. So, a large fraction of the overall mass is not required to be on the amplifiers to obtain wide low-frequency band gaps, provided that k_a/k is moderately large and θ is small. This is unlike obtaining wide low-frequency gaps via local resonators, which require heavy resonators that form a large fraction of the overall mass of their unit cell.

IV. CONCLUSIONS

Characteristics of the phononic band gaps generated by inertial amplification have been investigated in this work. First, a simple low-pass triangular truss structure was considered. It is shown that the addition of rigid amplification mechanisms to this structure does not change the wave

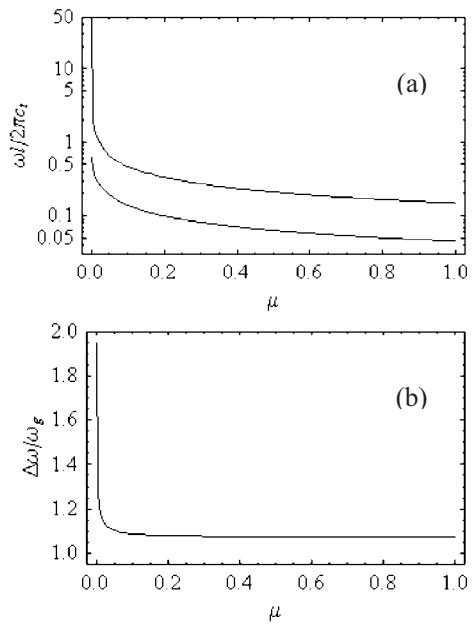

FIG. 13. (a) Upper and lower band gap limits of the first band gap in the lattice with inertial amplification for $k_a/k=10$ and $\theta=\pi/60$ as a function of mass fraction on amplifiers μ. (b) Normalized gap width as a function of μ.

speeds or the number of branches or its low-pass nature if the overall mass of the unit cell is kept constant. However, the rigid amplification mechanisms can reduce the highest frequency in the lattice considerably, provided that amplification is large and the mass fraction on amplifiers is not very small. Then, finite stiffness amplification mechanisms were considered. It is shown that the widest low-frequency band gaps are obtained when most of the mass within the lattice is concentrated on very stiff amplifiers that can generate large amplifications. However, with smaller mass fractions on amplifiers, wide low-frequency band gaps can still be obtained, provided that amplifiers are moderately stiff and can generate reasonably large amplifications. This is in contrast to obtaining wide low-frequency gaps via local resonators, which require heavy resonators that form a large fraction of the overall mass of their unit cell. Moreover, unlike Bragg scattering, wave speeds and the lattice constant do not limit how low a band gap can be placed. Hence, this alternative method of generating band gaps has benefits especially in the low-frequency ranges.

Attention was restricted to a two-dimensional lattice that has embedded inertial amplifiers. Adapting inertial amplification to three-dimensional lattices can be achieved by placing the described amplification mechanism on each edge of a three-dimensional truss structure. Although we considered a lumped parameter system in this paper, the principles of obtaining wide low-frequency band gaps in distributed parameter (continuous) systems via inertial amplification would be similar. Explicitly, the amplification mechanisms within these systems should be able to generate large amplifications and their resonance frequencies have to be high.

Physically realizing a lattice with inertial amplification is considered for future work. It is expected that the experimental response of the lattice at low frequencies would be similar to the computed response of its lumped parameter model with finite stiffness amplification mechanisms. Specifically, it would show a wide band gap upper bounded by the lowest resonance frequency of the amplifiers. However, a distributed parameter model would be required if the response at high frequencies is sought after.

APPENDIX A

In this appendix, we derive the dispersion equation of the lattice, i.e., Eq. (2). The springs are assumed to be linear, massless, and undamped; oscillations are assumed to be small. Hence, linear theory is applicable. The notation in deriving the equations will be similar to Martinsson and Movchan.[21]

The origin of the Cartesian coordinate system in Fig. 2(b) is at node 1. The lattice vectors are

$$\mathbf{t}^{(1)} = (l,0)^T, \quad \mathbf{t}^{(2)} = \left(\frac{1}{2}l, \frac{\sqrt{3}}{2}l\right)^T, \tag{A1}$$

where l is the lattice constant, which determines the size of the unit cell. The domain covered by the unit cell is denoted as $\mathbf{D}$. With integer translations of $\mathbf{D}$ along the lattice vectors, the plane $\mathbb{R}^2$ is covered, i.e.,

$$\mathbb{R}^2 = \bigcup_{\mathbf{n}\in\mathbb{Z}^2} (\mathbf{D} + \mathbf{T}\mathbf{n}), \quad \mathbf{T} = (\mathbf{t}^{(1)}, \mathbf{t}^{(2)}), \tag{A2}$$

where the integer pairs $\mathbf{n}=(n_1,n_2)^T$ specify each cell in the plane. In the lattice, nine different angles denoted by β_j for $j=1,2,\ldots,9$ are needed to define the forces between neighboring masses,

$$\beta_{1+3i} = \frac{\pi}{3}i, \quad \beta_{2+3i} = \theta + \frac{\pi}{3}i,$$

$$\beta_{3+3i} = -\theta + \frac{\pi}{3}(i+1), \quad i = 0,1,2. \tag{A3}$$

Moreover, some of these angles will also be used to define the coordinates of the nodes in $\mathbf{D}$, denoted by $\mathbf{x}^j$ for $j=1,2,\ldots,7$, and are given by

$$\mathbf{x}^1 = (0,0)^T, \quad \mathbf{x}^2 = \frac{l}{2}(1,\tan(\beta_2))^T,$$

$$\mathbf{x}^3 = \frac{l}{2}\left(\frac{\cos(\beta_3)}{\cos(\beta_2)}, \frac{\sin(\beta_3)}{\cos(\beta_2)}\right)^T,$$

$$\mathbf{x}^4 = \frac{l(\sqrt{3} - \tan(\beta_2))}{4}(\sqrt{3},1)^T,$$

$$\mathbf{x}^5 = \frac{l(\sqrt{3} + \tan(\beta_2))}{4}(\sqrt{3},1)^T,$$

$$\mathbf{x}^6 = l\left(1 + \frac{\cos(\beta_5)}{2\cos(\beta_2)}, \frac{\sin(\beta_5)}{2\cos(\beta_2)}\right)^T,$$

$$\mathbf{x}^7 = l\left(1, \frac{\sqrt{3} - \tan(\beta_2)}{2}\right)^T. \tag{A4}$$

The coordinates of the node j in cell $\mathbf{n}$, denoted by $\mathbf{x}^{(\mathbf{n},j)}$, are obtained as

$$\mathbf{x}^{(\mathbf{n},j)} = \mathbf{x}^j + \mathbf{T}\mathbf{n}. \tag{A5}$$

Furthermore, the displacement vector of the node j in cell $\mathbf{n}$ is denoted as

$$\mathbf{u}^{(\mathbf{n},j)} = (u_1{}^{(\mathbf{n},j)}, u_2{}^{(\mathbf{n},j)})^T. \tag{A6}$$

Now, by assigning to each β_j a unit vector

$$\mathbf{a}_j = (\cos(\beta_j), \sin(\beta_j))^T, \quad j = 1,2,\ldots,9, \tag{A7}$$

and defining $\mathbf{e}_1=(1,0)^T, \mathbf{e}_2=(0,1)^T$, the equations of motion for the case of harmonic oscillations (with circular frequency ω) can be written as

$$\omega^2 m\mathbf{u}^{(\mathbf{n},1)} = k\mathbf{a}_1\mathbf{a}_1^T(2\mathbf{u}^{(\mathbf{n},1)} - \mathbf{u}^{(\mathbf{n}-\mathbf{e}_1,1)} - \mathbf{u}^{(\mathbf{n}+\mathbf{e}_1,1)}) + k\mathbf{a}_4\mathbf{a}_4^T(2\mathbf{u}^{(\mathbf{n},1)} - \mathbf{u}^{(\mathbf{n}-\mathbf{e}_2,1)} - \mathbf{u}^{(\mathbf{n}+\mathbf{e}_2,1)}) + k\mathbf{a}_7\mathbf{a}_7^T(2\mathbf{u}^{(\mathbf{n},1)} - \mathbf{u}^{(\mathbf{n}-\mathbf{e}_1+\mathbf{e}_2,1)} - \mathbf{u}^{(\mathbf{n}+\mathbf{e}_1-\mathbf{e}_2,1)})$$
$$+ k_a\mathbf{a}_2\mathbf{a}_2^T(2\mathbf{u}^{(\mathbf{n},1)} - \mathbf{u}^{(\mathbf{n},2)} - \mathbf{u}^{(\mathbf{n}-\mathbf{e}_1-\mathbf{e}_2,7)}) + k_a\mathbf{a}_3\mathbf{a}_3^T(2\mathbf{u}^{(\mathbf{n},1)} - \mathbf{u}^{(\mathbf{n},3)} - \mathbf{u}^{(\mathbf{n}-\mathbf{e}_1-\mathbf{e}_2,6)}) + k_a\mathbf{a}_5\mathbf{a}_5^T(2\mathbf{u}^{(\mathbf{n},1)} - \mathbf{u}^{(\mathbf{n}-\mathbf{e}_1,6)} - \mathbf{u}^{(\mathbf{n}-\mathbf{e}_2,3)})$$
$$+ k_a\mathbf{a}_6\mathbf{a}_6^T(2\mathbf{u}^{(\mathbf{n},1)} - \mathbf{u}^{(\mathbf{n}-\mathbf{e}_1,5)} - \mathbf{u}^{(\mathbf{n}-\mathbf{e}_2,4)}) + k_a\mathbf{a}_8\mathbf{a}_8^T(2\mathbf{u}^{(\mathbf{n},1)} - \mathbf{u}^{(\mathbf{n}-\mathbf{e}_1,4)} - \mathbf{u}^{(\mathbf{n}-\mathbf{e}_2,5)}) + k_a\mathbf{a}_9\mathbf{a}_9^T(2\mathbf{u}^{(\mathbf{n},1)} - \mathbf{u}^{(\mathbf{n}-\mathbf{e}_1,2)} - \mathbf{u}^{(\mathbf{n}-\mathbf{e}_2,7)}),$$

$$\omega^2 m_a\mathbf{u}^{(\mathbf{n},2)} = k_a\mathbf{a}_2\mathbf{a}_2^T(\mathbf{u}^{(\mathbf{n},2)} - \mathbf{u}^{(\mathbf{n},1)}) + k_a\mathbf{a}_9\mathbf{a}_9^T(\mathbf{u}^{(\mathbf{n},2)} - \mathbf{u}^{(\mathbf{n}+\mathbf{e}_1,1)}),$$

$$\omega^2 m_a\mathbf{u}^{(\mathbf{n},3)} = k_a\mathbf{a}_3\mathbf{a}_3^T(\mathbf{u}^{(\mathbf{n},3)} - \mathbf{u}^{(\mathbf{n},1)}) + k_a\mathbf{a}_5\mathbf{a}_5^T(\mathbf{u}^{(\mathbf{n},3)} - \mathbf{u}^{(\mathbf{n}+\mathbf{e}_2,1)}),$$

$$\omega^2 m_a\mathbf{u}^{(\mathbf{n},4)} = k_a\mathbf{a}_8\mathbf{a}_8^T(\mathbf{u}^{(\mathbf{n},4)} - \mathbf{u}^{(\mathbf{n}+\mathbf{e}_1,1)}) + k_a\mathbf{a}_6\mathbf{a}_6^T(\mathbf{u}^{(\mathbf{n},4)} - \mathbf{u}^{(\mathbf{n}+\mathbf{e}_2,1)}),$$

$$\omega^2 m_a\mathbf{u}^{(\mathbf{n},5)} = k_a\mathbf{a}_6\mathbf{a}_6^T(\mathbf{u}^{(\mathbf{n},5)} - \mathbf{u}^{(\mathbf{n}+\mathbf{e}_1,1)}) + k_a\mathbf{a}_8\mathbf{a}_8^T(\mathbf{u}^{(\mathbf{n},5)} - \mathbf{u}^{(\mathbf{n}+\mathbf{e}_2,1)}),$$

$$\omega^2 m_a\mathbf{u}^{(\mathbf{n},6)} = k_a\mathbf{a}_5\mathbf{a}_5^T(\mathbf{u}^{(\mathbf{n},6)} - \mathbf{u}^{(\mathbf{n}+\mathbf{e}_1,1)}) + k_a\mathbf{a}_3\mathbf{a}_3^T(\mathbf{u}^{(\mathbf{n},6)} - \mathbf{u}^{(\mathbf{n}+\mathbf{e}_1+\mathbf{e}_2,1)}),$$

$$\omega^2 m_a\mathbf{u}^{(\mathbf{n},7)} = k_a\mathbf{a}_9\mathbf{a}_9^T(\mathbf{u}^{(\mathbf{n},7)} - \mathbf{u}^{(\mathbf{n}+\mathbf{e}_2,1)}) + k_a\mathbf{a}_2\mathbf{a}_2^T(\mathbf{u}^{(\mathbf{n},7)} - \mathbf{u}^{(\mathbf{n}+\mathbf{e}_1+\mathbf{e}_2,1)}). \quad \text{(A8)}$$

In Eq. (A8), any cell $\mathbf{n}+\mathbf{m}$, where $\mathbf{m}=(m_1,m_2)^T$ is an integer pair, corresponds to the cell obtained by m_1 translations along $\mathbf{t}^{(1)}$ and m_2 translations along $\mathbf{t}^{(2)}$ with respect to the cell $\mathbf{n}$. Assuming straight line wave fronts (analogous to plane waves in three dimensions), displacements at the cell $\mathbf{n}+\mathbf{m}$ are given by

$$\mathbf{u}^{(\mathbf{n}+\mathbf{m},j)} = e^{i\boldsymbol{\gamma}\cdot\mathbf{T}m}\cdot\mathbf{u}^{(\mathbf{n},j)}, \quad j=1,2,\ldots,7, \quad i=\sqrt{-1}, \quad \text{(A9)}$$

via Bloch's theorem.[18–20] In Eq. (A9), $\boldsymbol{\gamma}=(\gamma_1,\gamma_2)$ denotes the wave vector. By substituting Eq. (A9) into Eq. (A8), all the unknown displacements in Eq. (A8) can be written in terms of $\mathbf{u}^{(\mathbf{n},j)}$ for $j=1,2,\ldots,7$. By defining the 14×1 vector,

$$\mathbf{u}^{(\mathbf{n})} = ({u_1}^{(\mathbf{n},1)}, {u_2}^{(\mathbf{n},1)}, \ldots, {u_1}^{(\mathbf{n},7)}, {u_2}^{(\mathbf{n},7)})^T, \quad \text{(A10)}$$

the equations of motion can be compactly written as

$$\omega^2\mathbf{M}\mathbf{u}^{(\mathbf{n})} = \mathbf{K}(\boldsymbol{\gamma})\mathbf{u}^{(\mathbf{n})}, \quad \text{(A11)}$$

where the mass matrix $\mathbf{M}$ is a 14×14 diagonal matrix with the first two diagonal terms equal to m and the rest equal to m_a. The stiffness matrix $\mathbf{K}(\boldsymbol{\gamma})$ is obtained by arranging the right-hand sides of Eq. (A8) after substituting Eq. (A9). From Eq. (A11), we arrive at the dispersion equation of the lattice, i.e.,

$$\det(\mathbf{K}(\boldsymbol{\gamma}) - \omega^2\mathbf{M}) = 0. \quad \text{(A12)}$$

APPENDIX B

In this appendix, we give the derivation of Eq. (5). Note that if $k_a\to\infty$, all the nodal displacements can be obtained in terms of the displacements of the structural nodes, which are shown in Fig. 5. The displacement amplitudes of the masses at nodes 1, 4, and 5 is u. Due to symmetry, nodes 2, 3, 6, and 7 have equal displacement amplitudes. Consider node 2. The y components of the structural node displacements induce a displacement along the x axis with amplitude $u\tan(\theta)/2$, and the x components of the structural node displacements induce a displacement along the y axis with amplitude $\sqrt{3}u/(2\tan(\theta))$. Thus, the displacement amplitude of node 2 and of nodes 3, 6, and 7 is the sum of the squares of these two quantities in square root. Using the displacement amplitudes obtained above, the kinetic energy of the unit cell is given by

$$T = \frac{1}{2}(m+2m_a)\dot{u}^2 + \frac{1}{2}(4m_a)\left(\frac{3}{4\tan(\theta)^2} + \frac{\tan(\theta)^2}{4}\right)\dot{u}^2. \quad \text{(B1)}$$

In the lattice, the springs that form the edges of the unit cell are shared by the neighboring cells. Thus, half of the potential energy of these springs contributes to the potential energy within the unit cell. Due to symmetry, these springs have equal deformation amplitudes. Consider the spring at the bottom edge. Only the x components of the structural node displacements induce a deformation, which results in an amplitude of $\sqrt{3}u$. Moreover, there is no deformation in the spring that is in the middle of the unit cell. Then, within the unit cell, the potential energy is

$$V = 2\left(\frac{1}{2}k(\sqrt{3}u)^2\right). \quad \text{(B2)}$$

From Lagrange's equation,[22] i.e.,

$$\frac{d}{dt}\left(\frac{\partial T}{\partial\dot{u}}\right) - \frac{\partial T}{\partial u} + \frac{\partial V}{\partial u} = 0, \quad \text{(B3)}$$

the equation of motion for this mode is

$$\left[m_a \left(\frac{3}{\tan(\theta)^2} + \tan(\theta)^2 + 2 \right) + m \right] \ddot{u} + 6ku = 0. \quad \text{(B4)}$$

In Eq. (B4), the term that multiplies $\ddot{u}$ is the effective inertia of the unit cell. Given m and m_a, the effective inertia can be quite large by prescribing small values of θ. From Eq. (B4), ω_s is obtained as

$$\omega_s^2 = \frac{6k}{m_a \left(\frac{3}{\tan(\theta)^2} + \tan(\theta)^2 + 2 \right) + m}. \quad \text{(B5)}$$

*Corresponding author; cyilmaz@umich.edu

[1] L. Brillouin, *Wave Propagation in Periodic Structures: Electric Filters and Crystal Lattices* (McGraw-Hill, New York, 1946).
[2] M. M. Sigalas and E. N. Economou, Solid State Commun. **86**, 141 (1993).
[3] M. S. Kushwaha, P. Halevi, G. Martinez, L. Dobrzynski, and B. Djafari-Rouhani, Phys. Rev. B **49**, 2313 (1994).
[4] M. Kafesaki, M. M. Sigalas, and E. N. Economou, Solid State Commun. **96**, 285 (1995).
[5] M. S. Kushwaha, Int. J. Mod. Phys. B **10**, 977 (1996).
[6] I. E. Psarobas, N. Stefanou, and A. Modinos, Phys. Rev. B **62**, 278 (2000).
[7] O. Sigmund and J. S. Jensen, Philos. Trans. R. Soc. London, Ser. A **361**, 1001 (2003).
[8] M. I. Hussein, Ph.D. thesis, University of Michigan, 2004.
[9] M. S. Kushwaha, B. Djafari-Rouhani, L. Dobrzynski, and J. O. Vasseur, Eur. Phys. J. B **3**, 155 (1998).
[10] Z. Liu, C. T. Chan, and Ping Sheng, Phys. Rev. B **65**, 165116 (2002).
[11] M. S. Kushwaha, B. Djafari-Rouhani, and L. Dobrzynski, Phys. Lett. A **248**, 252 (1998).
[12] Z. Liu, X. Zhang, Y. Mao, Y. Y. Zhu, Z. Yang, C. T. Chan, and P. Sheng, Science **289**, 1734 (2000).
[13] C. Goffaux and J. Sanchez-Dehesa, Phys. Rev. B **67**, 144301 (2003).
[14] J. S. Jensen, J. Sound Vib. **266**, 1053 (2003).
[15] M. Hirsekorn, P. P. Delsanto, N. K. Batra, and P. Matic, Ultrasonics **42**, 231 (2004).
[16] W. G. Flannelly, U.S. Patent No. 3,322,379 (30 May 1967).
[17] C. Yilmaz and N. Kikuchi, J. Sound Vib. **293**, 171 (2006).
[18] C. Kittel, *Introduction to Solid State Physics* (Wiley, New York, 1966).
[19] N. W. Ashcroft and N. D. Mermin, *Solid State Physics* (Brooks-Cole, Belmont, MA, 1976).
[20] A. S. Phani, J. Woodhouse, and N. A. Fleck, J. Acoust. Soc. Am. **119**, 1995 (2006).
[21] P. G. Martinsson and A. B. Movchan, Q. J. Mech. Appl. Math. **56**, 45 (2003).
[22] L. Meirovitch, *Analytical Methods in Vibrations* (Macmillan, New York, 1967).